Modelling and Validation of a Switched Reluctance Motor Stator Tooth with Direct Coil Cooling

Jasper Nonneman[1,2], Stephan Schlimpert[3], Ilya T'Jollyn[1,2], Michel De Paepe[1,2]
[1]Department of Electromechanical, Systems and Metal Engineering, Ghent University, Sint-Pietersnieuwstraat 41, 9000 Ghent, Belgium
[2]Flanders Make@UGent – Core lab EEDT-MP
[3]Flanders Make, Core Lab MotionS, Gaston Geenslaan 8, 3001, Leuven, Belgium
Email: Jasper.Nonneman@UGent.be

ABSTRACT

This paper presents the modelling and validation of an advanced thermal lumped parameter (LP) model for a stator tooth of a switched reluctance motor (SRM) with a dry lateral slot cooling method. Standard and simple lumped parameter models for electric motors can insufficiently predict the temperature distribution within the components of the motor. In standard LP models, only several nodes are used to model each component, while more accurate models are needed to predict the effect of different cooling methods on the thermal performance of the motor without the need for experiments. A fully 3D thermal finite element (FE) model could be used but this would increase effort, complexity and computing time unnecessarily. Therefore, an advanced 3D LP model including the dry lateral slot cooling method was developed and validated based on experiments on a real stator tooth cooled with the modelled cooling method. The 3D LP model is extracted from a 2D FE radial simulation of the stator tooth and extended axially in 3D to include axial heat transfer. Experiments were performed with a setup consisting of one tooth of a SRM without rotor, but including stator iron, one winding and two triangular stainless steel tubes in the slots at both sides of the winding cooled by a 60/40% mixture by mass of water-glycol. The setup is equipped with several thermocouples integrated within the components to determine the component temperatures. Three inlet temperatures (20, 35 and 50°C) and four flow rates (2, 6, 9 and 13 l/min) of the coolant were tested at three different heat losses in the winding (10, 30 and 50 W). A comparison between the simulated and measured temperatures showed generally higher temperatures in the experiment. The presence of imperfections in the manufacturing of the experimental setup was determined as the cause of this offset. These imperfections result in lower material thermal conductivities and higher contact resistances than expected from scientific literature. After fitting those thermal properties on the measurements, similar simulated temperatures could be obtained as in the experiments.

KEY WORDS: Electric motor cooling, Direct coil cooling, Dry slot cooling, Contact resistance, Interface resistance, 2D Finite element, 3D lumped parameter model

NOMENCLATURE

A	Area (m²)
b	Constant array (W)
C	Heat capacity (J/kgK)
h	Convection coefficient (W/m²K)
k	Thermal conductivity (W/mK)
K	Thermal conductance (matrix) (W/K)
$\dot{Q}$	Heat transfer (W)
R	Thermal resistance (K/W)
Re	Reynolds number (-)
t	Time (s)
T	Temperature (array) (°C)
V	Volume flow rate (l/min)

Greek symbols

Δ	Difference
σ	Standard deviation

Subscripts

abs	absolute
amb	ambient
avg	average
c	coil, contact
exp	experiment
ext	external
in	inlet
i,j	node indices
mod	model
rel	relative

INTRODUCTION

Electrical alternatives to combustion engines in the transport sector become more and more popular. These electrified drivetrains, consisting of batteries, power electronics and an electric motor experience the trend to get more power dense. As a result, the cooling limit of the conventional cooling methods such as a jacket, starts to be reached and excessive temperatures are attained within the components of the drivetrain [1].

The most commonly used electric motor in these drivetrains is a Permanent Magnet Synchronous Motor (PMSM), but these make use of rare earth materials for the permanent magnets. A successfully proven alternative is a Switched Reluctance Motor (SRM), which does not use these rare earth materials and can attain similar rotational speeds, torque and efficiency [2]. A SRM consists of an iron laminated stator with copper windings and a laminated rotor. The temperature in the winding is mostly the bottleneck to go to higher power densities and peak powers in this type of motor because of the long thermal path from winding to jacket, the low thermal conductivity of the winding in radial and tangential direction [3] and the significant Joule heating in the wires.

As a result, more effective cooling methods are needed for the windings specifically to increase the power density further. One of the possibilities is to cool the winding more directly within the slot. Within scientific literature, several possibilities of direct coil cooling have been studied.

Schiefer et al. [4] both experimentally and numerically studied the direct coil cooling method applied to the concentrated windings of an interior permanent magnet synchronous machine (IPMSM). In this study, round wires

were replaced by flat wires leaving several gaps in the slot that can be used as cooling channels. The channels were sealed and created by potting using the lost-wax casting method. Rhebergen et al. [5], Sixel et al. [6], Semidey et al. [7], Fairall et al. [8], and Ibrahim et al. [9] investigated metallic or plastic tubes inserted within the slot in direct contact with the coil. Rhebergen et al. [5] used a plastic material to avoid electromagnetic and implementation issues. Sixel et al. [6] 3D printed a channel that fits the otherwise unused space between double layer concentrated windings. Semidey et al. [7] investigated the effect of a microfeature enhanced channels, which resulted in very high heat transfer coefficients. In these scientific studies, the great potential of the implementation of direct coil cooling is shown. Fairall et al. [8] and Ibrahim et al. [9] studied the effect of the insertion of the tube material into the slot on the eddy current loss in a Switched Reluctance Motor. It is found in these studies that plastic materials do not cause additional losses and that the losses for a stainless steel tube material are acceptable.

The influence on the motor temperature of the different methods used in the studies is very difficult to compare based on the described results, because deviating geometries and boundary conditions were used. A numerical model can be used to make a comparison of the various methods, which can be a lumped parameter model (LPM) or finite element model (FEM) with or without computational fluid dynamics (CFD). LP models are fast and simple, but are less accurate than FEM and CFD, while the latter increase the complexity and computational time of the simulations [10]. In a previous publication an advanced thermal lumped parameter (LP) model for a switched reluctance motor (SRM) with a dry lateral slot cooling method was constructed based on a 2D FE simulation, which combines the benefits of a LP and FE model [11].

The objective of this paper is to validate the developed model based on experimental measurements on a SRM stator tooth with direct coil cooling. Only one stator tooth was used for the experiments and validation due to symmetry of the motor and to limit the complexity of the experimental setup (no rotating machine). The experimental setup used for these measurements was designed and build within the framework of the ICON Hipercool project.

Hereafter the used motor geometry is described and an overview of the developed lumped parameter model is given. Further, the experimental setup and test section are shown which are used for the measurements. These measurement results are then compared to the simulated data based on motor thermal properties from scientific literature. At last a best fit of the motor thermal properties is made with the onto the measurement results.

GEOMETRY DESCRIPTION

The motor type studied within this paper is a switched reluctance motor as shown in Figure 1. It consists of a laminated stator that generates a magnetic field using power delivered to the stator coils. The rotor only consists of iron laminations and tends to go to a minimum state of reluctance. The use of preformed concentrated stator windings (which have a high filling factor) leaves a triangular space in the slot between the adjacent windings and stator yoke due to the conical shape of the slot, which can be used to insert a cooling channel. Filling the slot completely with wires is also possible but this typically results in a lower filling factor. In this case, some space should be sacrificed for cooling. Within this paper, preformed stator windings will be studied and as a result, triangular tubes can be inserted within the slot.

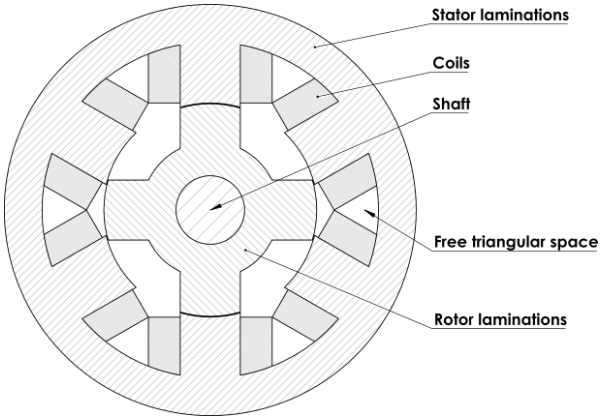

Figure 1: Typical sectional view of a 6/4-SRM.

The tube should fill the space within the gap completely to assure a good thermal contact between tube, stator iron and coils. Therefore a triangular shaped tube will be used. The thermal resistance of the tube should be as low as possible to avoid a high temperature drop over the tube wall. Therefore, a metallic tube is preferred compared to a plastic material, because the thermal conductivity and strength are usually lower. As was investigated by Ibrahim et al. [9], the additional eddy current losses within stainless steel tubes are neglectable and therefore stainless steel will be used as tube material within the validation measurements. The motor parameters of the used motor geometry are shown in Table 1.

Table 1: Motor parameters of the validation geometry [9].

Stator/rotor poles	6/4
Axial active length	80 mm
Shaft diameter	20 mm
Rotor outer diameter	62 mm
Stator outer diameter	120 mm
Airgap thickness	0.25 mm
Yoke thickness	11 mm
Pole width	17.5 mm
Rated speed	3000 rpm
Rated power	3 kW

LUMPED PARAMETER MODEL

The model has already been described elaborately in the publication of Nonneman et al. [11]. Only an overview of the model principle will be described within this paper and a more detailed description of the dry slot cooling method will be discussed. More details on the model principle and implementation can be found within [11].

Overview

A generic model has been developed to be able to study the impact of advanced liquid cooling methods and the interaction between the different methods. The developed advanced thermal lumped parameter (LP) model uses a combination of a

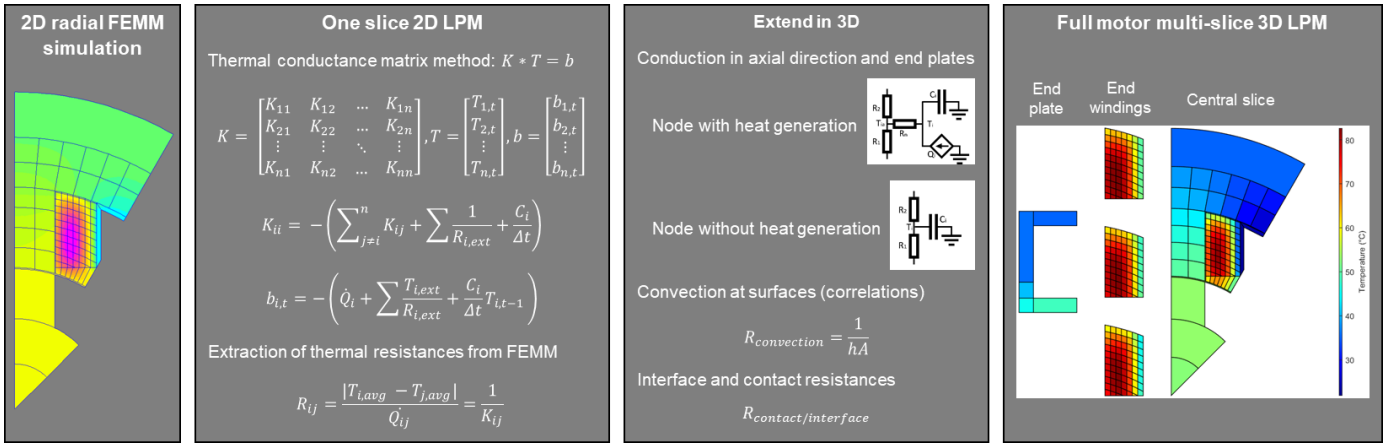

Figure 2: 3D LP model flowchart (K thermal conductance matrix; T array of node temperatures; b dependent on heat input, heat transfer to external media and temperature at previous time iteration t; i and j represent nodes; R_{ij} thermal resistance and K_{ij} thermal conductance between these nodes; $\dot{Q}_i$ heat coming into node i; $R_{i,ext}$ thermal resistance to the external temperature $T_{i,ext}$ of the medium; C_i heat capacity of node i; Δt time step, T_{avg} average node temperature in FEMM, h convection coefficient, A heat transfer area).

finite element (FE) model and a LP model. A flow chart of the model is shown in Figure 2.

A 2D FEM simulation is performed of an axisymmetric slice of the motor to account for the complex geometry and high thermal gradients in this direction. For the convective boundary conditions, correlations from scientific literature are used. From this 2D FE simulation of the radial slice, a lower order LPM is extracted. A coarse discretization is put onto the 2D slice to be able to calculate local temperatures, with more nodes for components where a high 2D thermal gradient occurs compared to other components with lower thermal gradients. This is mainly necessary for the coil, since high thermal gradients are evident due to the low thermal conductivity and high heat generation. To assure a smooth transition from coil to the other components, the liners around the coil should also be meshed. In addition, the stator laminations can be meshed as well.

Within the axial direction, the methods of a typical LPM are used to extend the model in 3D. To include the axial gradient in the motor, the motor is split into three main parts (see Figure 3): the active part (green), the end winding part (red) and the end plates (black) which include a part of the housing, flanges, bearings and a part of the shaft. When higher axial gradients occur as for example with end winding cooling, the accuracy of the model can be improved with different axial slices of the active and end winding part.

Direct coil cooling – dry slot

The convective heat transfer coefficient within the triangular channel is calculated based on correlations from scientific literature, dependent on the Reynolds number Re. In the laminar region, the fully developed Nusselt number for the triangular channel is dependent on the amount of sides of the triangular channel that are heated. The data of Schmidt et al [12] is used to calculate the Nusselt number for fully developed flow for a triangular channel. For laminar developing flow in a triangular channel, the correlation of Shah and London [22] is used to calculate the local Nusselt number, for simultaneously developing flow with the uniform heat flux boundary condition, which is the best approximation. In the turbulent region, the correlation of Gnielinski [13] is used to calculate the fully developed Nusselt number. To take into account the development of the flow in the turbulent region the correction factor of El-Arabi et al. [14] is used for simultaneously developing turbulent flow. In the region of transitional flow a linear interpolation between the Nusselt numbers at $Re = 2300$ and $Re = 4000$ is used [15]. Depending on the model inputs, the correct correlation is chosen within the model.

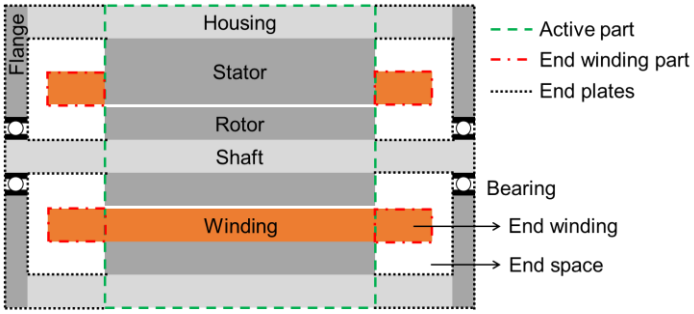

Figure 3: Motor region definition.

EXPERIMENTAL SETUP

Overview

The stator tooth equipped with direct cooling is experimentally measured within an existing experimental setup. The experimental setup is designed in a way that different drive train components (power electronics; motor tooth; DC-DC charger; etc.) can be experimentally investigated in an automatic, fast, efficient and accurate manner due to a plug and play design with respect to the test section [16]. The test section is cooled with a 60/40% by mass mixture of water-glycol that is stored within a reservoir. A gear pump has the function to circulate the fluid around within the fluid conditioning part, which is shown on Figure 4. Conditioned fluid is available in a reservoir from where it flows to the test section where heat is extracted. The hot fluid then flows back to the reservoir after passing through the chiller tank where it is cooled to the desired temperature. Heat losses from the fluid to the ambient are minimized by maintaining the ambient temperature as close as possible to the fluid temperature with an HVAC system.

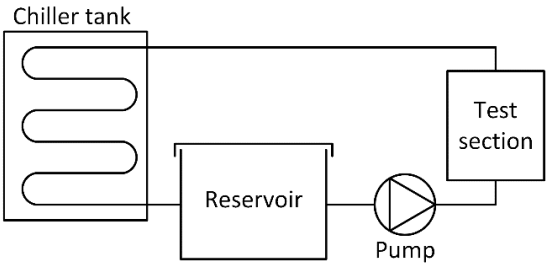

Figure 4: Overview of the experimental setup.

Test section

The test section, shown in Figure 5, consists of one tooth of a SRM without rotor, but including stator iron, one impregnated winding and two triangular stainless steel tubes in the slots at both sides of the winding. A Nomex liner is present between the coil and stator iron pole and yoke.

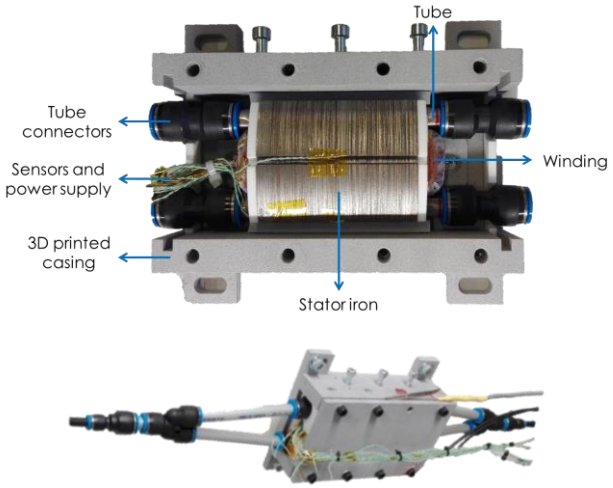

Figure 5: Picture of test section overview (top) and test section installed in setup with casing closed (bottom).

The tubes are connected in parallel and cooled with the conditioned water-glycol mixture of the conditioning circuit. The triangular tubes are formed out of circular tubes with a triangular mold. As a result, the corners of the tube are not perfectly sharp but slightly bended, originating from the circular tube Figure 6 shows half of the experimental setup with the components indicated in detail and where the tubes are drawn as perfectly sharp.

To improve the thermal contact between the tube-coil and tube-stator iron yoke, thermal paste is applied on these two contact surfaces as shown in Figure 6. Next to the resistance of the interface materials (Nomex and thermal paste), also contact resistances are present between the coil and Nomex, Nomex and stator pole/yoke, tube and coil and tube and stator yoke. The location of these contact resistances is also shown in Figure 6. The exact thermal properties of the used materials and contacts could not be measured and therefore, properties from datasheets and scientific literature were used as inputs for the model. The used values are shown in Table 2.

A 3D printed casing out of low conductive material (polyamide) was manufactured to be able to keep the components together and to limit heat losses from the test section to the environment.

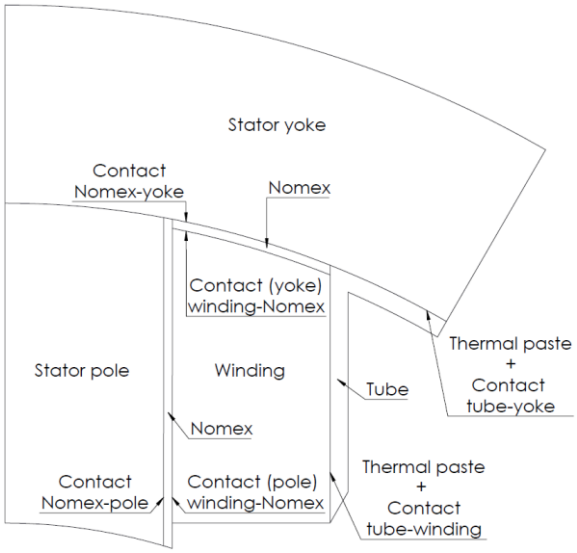

Figure 6: Sectional drawing of half of the experimental setup (test section) with the components indicated.

Table 2: Thermal material properties from scientific literature.

Property	Value
$k_{stator\ iron,radial}$	$20.6\ W/mK$ [17]
$k_{stator\ iron,axial}$	$1.2\ W/mK$ [17]
$k_{coil,radial}$	$1.03\ W/mK$ [18]
$k_{coil,axial}$	$250\ W/mK$ [18]
k_{tube}	$14.3\ W/mK$ [19]
k_{Nomex}	$0.1\ W/mK$ [4]
$R_{contact,coil-Nomex}$	$0.0018\ m^2K/W$ [20]
$R_{contact,Nomex-pole/yoke}$	$0.0006\ m^2K/W$ [20]
$R_{contact,tube-coil}$	$0.0018\ m^2K/W$ [20]
$R_{contact,tube-yoke}$	$0.0006\ m^2K/W$ [20]

Sensors

Several sensors are included within the setup to determine the thermal performance of the cooling method and to validate the model. Two PT100 temperature sensors measure the fluid temperature at the inlet and outlet of the test section. An ultrasonic flow meter measures the volumetric flow rate through the setup. The electrical DC current supplied to the winding to dissipate the necessary heat is determined by measuring the voltage and current. The uncertainty of the electric power measurement can be determined based on the uncertainty on the voltage and current measurement.

Nineteen K-type thermocouples are distributed within the stator tooth to map the temperature distribution and temperature drops over the interfaces as complete as possible. Figure 7 shows the location of the temperature sensors. The fluid enters the tubes at the side of slice A. Sensors 1 and 2 measure the tube temperature at the interface between tube and coil. Sensors 3-9 measure the coil temperature at different locations and sensors 10-19 measure the iron temperature at different locations. An overview of the range and uncertainty of the sensors within the setup is shown in Table 3.

Due to the difficulty of positioning the thermocouples accurately, the actual location can slightly deviate from the intended location. The hot junction of thermocouples located at the interface of two components can be in a better thermal

contact with one of the two components and thus measure only one of the two component temperatures, or measure an average of the two components. As a result, it is expected that higher deviations between model and experiment compared to the measurement uncertainty will appear for some of these sensors.

Table 3: Range and uncertainty of the sensors.

Sensor	Range	Uncertainty
PT100	-50…120°C	±0.15°C
K-type thermocouple	-50…250°C	±1°C
Ultrasonic flow meter	0.3…21 l/min	±1% ±0.014 l/min
Current	0…75A	±1%
Voltage	0…200V	±1%
Electric power	-	±2.1%

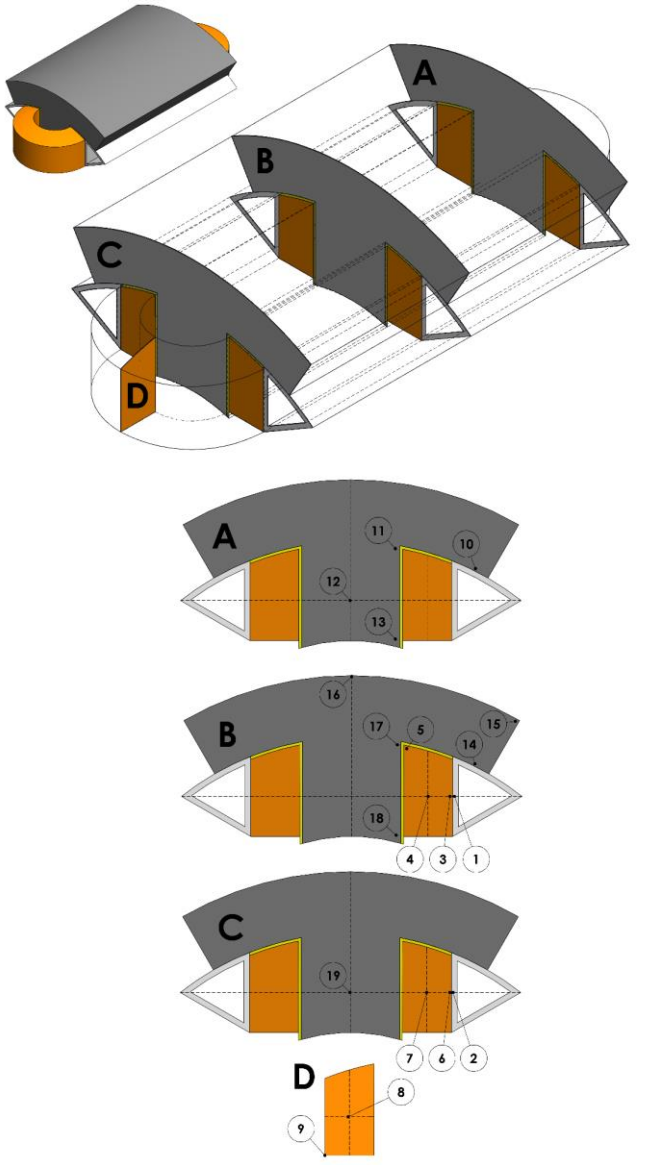

Figure 7: Thermocouple locations in the stator tooth setup with the slices A, B and C in the active part, and slice D in the end winding part.

Measurement plan and procedure

Measurements were performed for three fluid inlet temperatures (20°C, 35°C and 50°C) which are common in electric vehicles. To study the influence of the convective heat transfer coefficient, four different flow rates of the coolant were investigated (2, 6, 9 and 13 l/min) at three different heat losses in the winding (10, 30 and 50 W).

The following automated procedure was followed:

- Set a certain fluid inlet temperature along with the corresponding lab temperature (T_{amb} = 20°C for T_{in} = 20°C; T_{amb} = 28°C for T_{in} = 35 and 50°C).
- Run for 4h at the highest flow rate without heat losses in the winding to get the chiller tank and reservoir to a stable temperature.
- Start the test in order of decreasing flow rate and for every flow rate an increasing heating power.
- Measure one stable setpoint for a period of 10 min to get steady state values and limit the measurement noise.

Between every other heat loss setpoint, there was a stabilization time of 30 min, which was enough due to the low thermal inertia of the test stator tooth and small steps in the setpoints. Between different setpoints of the flow rate, a stabilization time of 10 min was used. One complete test procedure for one fluid temperature ($\sim 13h$) is fully automated with the above mentioned stabilization times, such that no deviations between the different fluid temperature setpoints are expected.

MEASUREMENT RESULTS AND VALIDATION

Next to the measured temperatures, the temperatures are also simulated with the 3D LP model which was described within the section 'Lumped parameter model' and of which an overview is shown in Figure 2. These simulations are based on the same inputs as in the experiment (inlet temperature, flow rate and heat loss). Within this section, the measured temperatures are shown in combination with these simulated temperatures.

Comparison of measurements with simulations based on thermal properties from scientific literature

A comparison of the simulated and measured temperatures for every setpoint subtracted by the inlet temperature of the fluid is shown in Figure 8. In this figure, the full black line shows the perfect match between model and experiment, while the dotted black lines indicate the range with a deviation of ±10°C. The light grey dots indicate the tube temperatures, orange dots the coil temperatures and dark grey dots the iron temperatures. The figure shows that in general the simulated temperatures underestimate the measured temperatures, certainly for the highest temperatures measured by sensor 4, 7 and 8, which are located in the center of the coil.

The measured and simulated temperatures for the case $Q_c = 50\ W$, $T_{in} = 20.6\ °C$ and $V = 12.7\ l/min$ are shown in Table 4. This specific case was selected because the influence of the convection in the channel is the smallest here (highest convection coefficient) and the highest temperature differences are obtained (highest heat losses), while none of the measured temperatures exceed the maximum temperature (lowest inlet temperature). The absolute and relative difference between the

modelled T_{mod} and measured temperature T_{exp} are calculated as:

$$\Delta T_{abs} = T_{mod} - T_{exp}$$
$$\Delta T_{rel} = \frac{T_{mod} - T_{exp}}{T_{exp} - T_{in}}$$

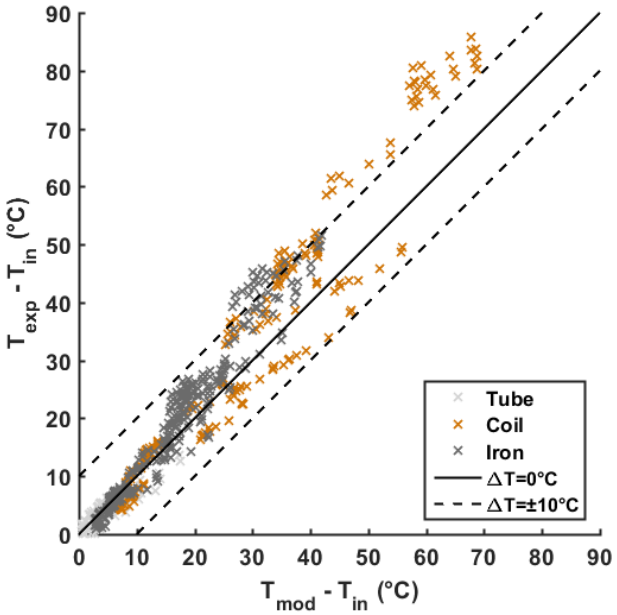

Figure 8: Comparison of the simulated and measured temperatures for the parameters from literature.

Table 4: Measured and simulated temperatures for the case $Q_c = 50\ W$, $T_{in} = 20.6\ °C$ and $V = 12.7\ l/min$ with inputs from literature (all values in °C, except the last column in %).

Location		Experiment	Model	ΔT_{abs}	ΔT_{rel}(%)
Tube	1	25.0	24.9	-0.1	-3.5
	2	25.7	25.4	-0.2	-4.6
Coil	3	57.0	52.0	-5.0	-13.8
	4	101.2	78.5	-22.7	-28.2
	5	82.1	64.3	-17.8	-29.1
	6	50.8	56.9	6.1	20.3
	7	98.7	79.0	-19.7	-25.3
	8	97.6	79.3	-18.3	-23.8
	9	64.2	65.7	1.5	3.5
Iron	10	33.6	35.6	1.9	15.0
	11	62.1	47.8	-14.3	-34.7
	12	59.3	50.0	-9.3	-24.2
	13	61.9	52.2	-9.7	-23.6
	14	39.9	36.2	-3.7	-19.1
	15	44.9	39.0	-5.9	-24.5
	16	49.2	45.3	-3.8	-13.5
	17	56.1	47.6	-8.5	-24.1
	18	65.4	51.7	-13.7	-30.7
	19	66.0	50.8	-15.3	-33.7

For this case the maximum temperature is measured by sensor 4 and is underestimated with ΔT_{abs}=22.7°C by the model, which is 28.2% lower than the measured value. The mean value of the relative difference ΔT_{rel} on the maximum temperature of each setpoint is -21.4%.

The cause is the presence of imperfections in the manufacturing of the experimental setup. Some of these imperfections are illustrated in Figure 9 and summarized here:

- The triangular tube has rounded edges and as a result, gaps appear between the tube-coil and tube-stator.
- The coil shape does not perfectly fit the slot space.
- The coil impregnation was not perfectly done: there were still airgaps present within the coil and at the interfaces.

As a result, the thermal properties from scientific literature as written in Table 2 do not properly predict those in the experimental setup.

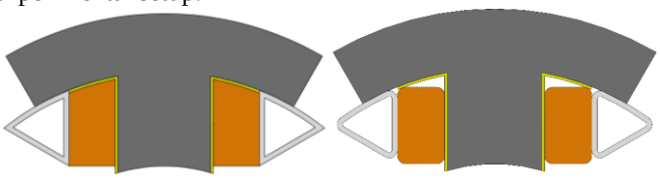

Figure 9: Perfectly manufactured tooth (left) imperfections (right).

This discrepancy between model and experiment can be quantified with the sum of squares SS of the temperature difference between model and experiment. The sum of squares can then be used to calculate the standard deviation σ between model and experiment, which both can be calculated as:

$$SS = \sum_{i=1}^{N} \left(T_{mod,i} - T_{exp,i}\right)^2$$
$$\sigma = \sqrt{\frac{SS}{N-1}}$$

With N the amount of temperature measurements (N=19). When using the thermal properties from literature for the measurement point of Table 4, a standard deviation of $\sigma = 11.9°C$ is obtained between model and experiments.

The influence of the fluid flow rate is shown in Figure 10. The figure shows the spreading of the temperature difference between model and experiment for the temperatures in the tube, coil and iron. The temperatures measured by sensor 1 and 2 (tube) are independent of the inputs of the model (Table 2), but are dependent on the calculated convection coefficient. Figure 10 shows that the difference in tube temperature between model and experiment in light grey. It is seen that the range decreases with increasing flow rate, which is caused by the higher convection coefficient at higher flow rates, resulting in a smaller temperature drop due to convection.

Taking into account the measurement error of the thermocouples, PT100 and heat losses from PT100 measurement at the inlet to the tube inlet, the difference $\Delta T_{mod-exp}$ is within the measurement uncertainty for the highest flow rates (9.3 and 12.8 l/min). For the lowest flow rates (2 and 5.7 l/min) it is generally higher than zero. Knowing that the lowest flow rate (2 l/min) is within the laminar region and the second flow rate (5.7 l/min) within the transitional region, it is presumed that the correlations within the laminar and transitional region slightly underestimate the heat transfer coefficient in the experiment. This enhancement of the heat transfer in the experiment compared to the calculated heat transfer coefficient by the correlation for simultaneously

developing laminar flow, is caused by the vorticity induced by the connectors and bend before the tube inlet. The effect of the connectors and bend on the heat transfer is relatively smaller within the turbulent region.

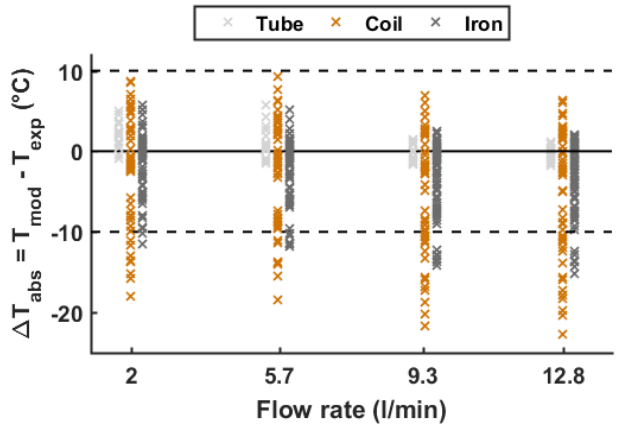

Figure 10: Influence of the flow rate on $\Delta T_{mod-exp}$ for the parameters from literature.

Estimation of thermal properties in the experimental setup

The previous analysis shows a discrepancy between the model and measured results caused by imperfections within the experimental setup. To find out how much the thermal properties of the tooth setup differ from the values from scientific literature of Table 2, a numerical best fit search of the thermal properties should be done, based on the experimental measurement results. The resulting thermal properties of the best fit can be compared to the values from scientific literature and the most important contributors to the under prediction of the temperatures by the model can then be identified.

The best fit search was done for the case with the highest heating power (highest temperature differences), highest flow rate (smallest influence of convection coefficient) and lowest inlet temperature (such that highest temperature within the setup is acceptable). Not every parameter of the table is included in the fitting to prevent overfitting of the parameters on the experiment. The thermal conductivity of the tube is excluded from the fitting because the temperature difference for sensor 1 and 2 between model and experiment is within the measurement uncertainty and the influence of the thermal conductivity of the tube is small within its possible range. Further the thermal conductivity of the coil and stator in axial direction are excluded, since there is no big and consistent temperature deviation in this direction. The thermal conductivity of the Nomex is also excluded, otherwise no unique solution can be found since the contact resistances compensate the changes in conductivity of the Nomex material (they are connected in series). Further, the contact resistances between coil-Nomex and Nomex-iron are also in series so that no unique solution can be found. These two resistances are therefore summed up as one parameter within the fitting. As a result, six parameters have to be fitted onto the experimental measurements.

The actual fitting is done by searching the combination of the selected input parameters of the model for which the sum of squares of the temperature difference between model and experiment is the least. Practically the LPM is re-simulated for various combinations of these input parameters and the resulting temperatures are compared with the measured temperatures by calculating the sum of squares. The minimum of the latter is then selected as the best fit of the thermal properties. The Matlab function 'fminsearchbnd' is used to search this minimum, which is a nonlinear programming solver that searches for the minimum of a problem within certain bounds [21].

After fitting the selected thermal properties, the values as shown in Table 5 (column 'fitted') result in the minimum sum of squares of the difference between model and experiment. In the last column of Table 5, the deviations in percentage from those out of literature are calculated. The thermal conductivity of the stator iron material is estimated to be 37% lower than the average value found in the literature. The conductivity of the coil in radial direction is 53% lower than the value from literature, but this is caused by the impregnation which was not perfectly done. The remaining gaps in the coil cause a bad thermal contact between the wires and result in a lower equivalent thermal conductivity in radial direction. The value obtained is comparable to the measured values in the literature for non-infiltrated coils [18].The contact resistances from coil to pole and coil to tube are slightly were slightly overestimated (respectively 23% and 39%) but the values are in the same order of magnitude. The value of the contact resistance from coil to yoke is estimated to be much higher in the setup than expected from literature (1804%), but this could be expected due to the big airgap between coil and yoke as illustrated in Figure 9. The contact resistance between tube and yoke is slightly higher in the experiment (38%), because the tube does not follow the curve of the stator iron well, leaving a small gap behind which was filled with thermal paste.

Table 5: Literature and fitting parameters.

Property	Literature	Fitted	Δ (%)
$k_{iron,radial}\left(\frac{W}{mK}\right)$	20.6	12.93	-37
$k_{coil,radial}\left(\frac{W}{mK}\right)$	1.03	0.486	-53
$R_{c,coil-Nomex+Nomex-pole}\left(\frac{m^2K}{W}\right)$	0.0024	0.00186	-23
$R_{c,coil-Nomex+Nomex-yoke}\left(\frac{m^2K}{W}\right)$	0.0024	0.0457	+1804
$R_{c,tube-coil}\left(\frac{m^2K}{W}\right)$	0.0018	0.0011	-39
$R_{c,tube-yoke}\left(\frac{m^2K}{W}\right)$	0.0006	0.00083	+38

Comparison of measurements with simulations based on fitted thermal properties

In Figure 11 the comparison of the simulated and measured temperatures is redone for every setpoint based on the fitted input parameters from Table 5. The difference between model and experiment is now much closer to the $\Delta T = 0$ line compared to Figure 8 and all point are within the $\pm 10°C$ range.

The measured and simulated temperatures for the case $Q_c = 50\ W$, $T_{in} = 20.6\ °C$ and $V = 12.7\ l/min$ are again shown in Table 6 but now with the fitted parameters. The standard deviation is now reduced to $\sigma = 3.3°C$, which is 3.6 times smaller than the standard deviation with the thermal properties from literature ($\sigma = 11.9°C$). The maximum temperature measured by sensor 4 is now underestimated with 1.5°C by the

model, which is only 1.9% lower than the measured value. The mean value of the relative difference ΔT_{rel} on the maximum temperature of each setpoint is now reduced to 6.2%.

Some of the deviations are still high (sensor 3, 6, 10, 11, 14), but this is presumably caused by the earlier mentioned reasons (difficulty of positioning the thermocouples accurately and measurements at the interface of two components). Further, the temperatures at the location of these sensors are not crucial since they are not the maximum temperatures.

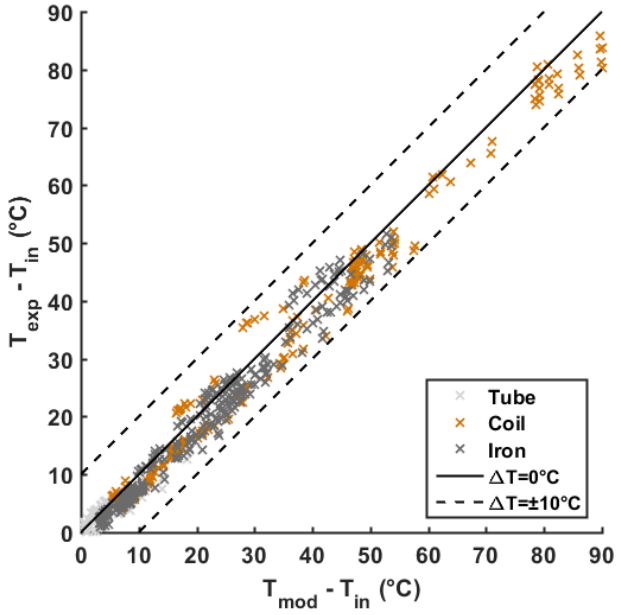

Figure 11: Comparison of the simulated and measured temperatures for the fitted parameters.

Table 6: Measured and simulated temperatures for the case $Q_c = 50\ W$, $T_{in} = 20.6\ °C$ and $V = 12.7\ l/min$ with inputs from fitting (all values in °C, except the last column in %).

Location		Experiment	Model	ΔT_{abs}	ΔT_{rel}(%)
Tube	1	25.0	25.0	0.0	0.0
	2	25.7	25.8	0.1	3.0
Coil	3	57.0	49.4	-7.5	-20.8
	4	101.2	99.7	-1.5	-1.9
	5	82.1	81.7	-0.5	-0.8
	6	50.8	55.8	5.0	16.5
	7	98.7	99.8	1.1	1.5
	8	97.6	99.9	2.4	3.1
	9	64.2	67.1	2.9	6.8
Iron	10	33.6	37.5	3.9	30.3
	11	62.1	57.4	-4.7	-11.4
	12	59.3	61.5	2.2	5.6
	13	61.9	65.5	3.6	8.9
	14	39.9	38.2	-1.7	-8.8
	15	44.9	42.1	-2.7	-11.4
	16	49.2	52.6	3.4	12.0
	17	56.1	56.8	0.8	2.2
	18	65.4	64.5	-0.9	-2.1
	19	66.0	62.1	-3.9	-8.6

Figure 12 shows the influence of the flow rate on the absolute temperature difference between model and experiment for the fitted parameters. The same conclusion and cause as Figure 10 is valid here. A higher convection coefficient in the model for the lowest flow rates would also improve the prediction of the coil and iron temperatures.

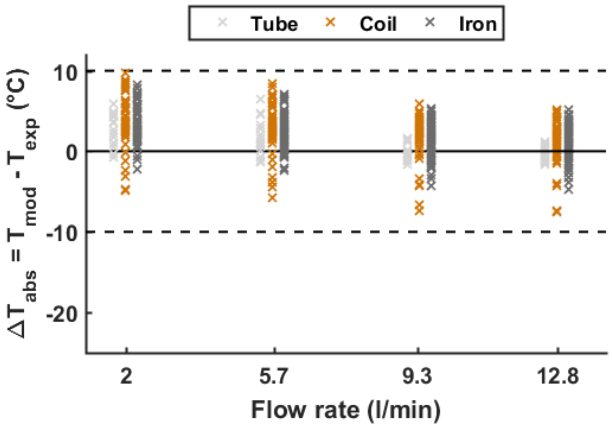

Figure 12: Influence of the flow rate on $\Delta T_{mod-exp}$ for the fitted parameters.

CONCLUSION

The dry direct coil cooling method was experimentally investigated on a SRM stator tooth setup equipped with 19 thermocouples distributed over the test section. These measurements were performed with a 60/40% mixture by mass of water-glycol flowing through triangular stainless steel tubes within the slot at different inlet temperatures and flow rates. The heat dissipation within the stator coil was also varied.

The measurements from the experimental setup were used to validate an advanced LP model including the dry lateral slot cooling method that was previously developed. This 3D LPM combines the benefits of a LP model (simple and fast) with the benefits of a FE model (accurate and detailed). When using thermal properties for the materials and contact resistances from literature as inputs for the model, the model generally underestimates the measured temperatures, with a mean relative difference on the maximum temperature of each setpoint of -21.6% and a standard deviation of 11.9°C. The cause are imperfections in the manufacturing of the tooth setup, leaving gaps behind between the different components. These gaps are low thermally conductive, resulting in high thermal contact resistances and low equivalent thermal conductivities of the materials.

By fitting the thermal properties within the 3D LP model on the measurement results, an estimation of these parameters for the experimental setup was obtained. The deviation of the fitted thermal properties compared to the values from scientific literature was lower than 50%, expect for the contact resistance between coil and stator yoke. The latter is much higher due to the fact that the coil shape does not perfectly fit the slot space, leaving a big airgap behind.

After re-simulation of the temperatures with the 3D LPM based on the fitted thermal properties, a standard deviation between model and experiment of 3.3°C was attained, which is 3.6 times smaller compared to simulations based on the scientific literature inputs. With these fitted thermal properties, the mean relative difference on the maximum temperature of

each setpoint could be reduced to 6.2%, with the absolute difference in the range -1.5°C → 6°C, which is acceptable.

This work shows that the advanced 3D LP model is capable of predicting the maximum motor temperatures within acceptable ranges when the thermal properties can be determined properly. The latter would have been the same issue if FEM or CFD would have been used and as a result, similar differences would occur. Therefore, it is concluded that the proposed advanced LPM is an efficient and accurate method against FEM and CFD.

Acknowledgments

This research was supported by Flanders Make, the strategic research centre for the manufacturing industry, and the HERMESFONDS in the framework of the Hipercool project (HBC.2016.0463).

References

[1] M. Popescu, D. A. Staton, A. Boglietti, A. Cavagnino, D. Hawkins, and J. Goss, "Modern heat extraction systems for power traction machines—A review," *IEEE Transactions on Industry Applications*, vol. 52, pp. 2167-2175, 2016.

[2] S. Haghbin, A. Rabiei, and E. Grunditz, "Switched reluctance motor in electric or hybrid vehicle applications: A status review," in *2013 IEEE 8th Conference on Industrial Electronics and Applications (ICIEA)*, 2013, pp. 1017-1022.

[3] C. Tighe, C. Gerada, and S. Pickering, "Assessment of cooling methods for increased power density in electrical machines," in *2016 XXII International Conference on Electrical Machines (ICEM)*, 2016, pp. 2626-2632.

[4] M. Schiefer and M. Doppelbauer, "Indirect slot cooling for high-power-density machines with concentrated winding," in *2015 IEEE International Electric Machines & Drives Conference (IEMDC)*, 2015, pp. 1820-1825.

[5] C. Rhebergen, B. Bilgin, A. Emadi, E. Rowan, and J. Lo, "Enhancement of electric motor thermal management through axial cooling methods: A materials approach," in *2015 IEEE Energy Conversion Congress and Exposition (ECCE)*, 2015, pp. 5682-5688.

[6] W. Sixel, M. Liu, G. Nellis, and B. Sarlioglu, "Cooling of Windings in Electric Machines via 3D Printed Heat Exchanger," in *2018 IEEE Energy Conversion Congress and Exposition (ECCE)*, 2018, pp. 229-235.

[7] S. A. Semidey and J. R. Mayor, "Experimentation of an electric machine technology demonstrator incorporating direct winding heat exchangers," *IEEE Transactions on Industrial Electronics*, vol. 61, pp. 5771-5778, 2014.

[8] E. Fairall, C. Rheberhegen, E. Rowan, J. Lo, B. Bilgin, and A. Emadi, "Maximizing thermal effectiveness and minimizing parasitic loss in a liquid cooled switched reluctance machine," in *2016 IEEE Transportation Electrification Conference and Expo (ITEC)*, 2016, pp. 1-7.

[9] M. N. F. Ibrahim and P. Sergeant, "Prediction of Eddy Current Losses in Cooling Tubes of Direct Cooled Windings in Electric Machines," *Mathematics*, vol. 7, p. 1096, 2019.

[10] J. Pierre-Olivier and L. B. Jean, "HEAT TRANSFER IN ELECTRIC MACHINES," 2017.

[11] J. Nonneman, N. Clarie, I. T'Jollyn, S. Schlimpert, P. Sergeant, and M. De Paepe, "Advanced lumped parameter model for switched reluctance motors with high performance cooling," in *International Heat Transfer Conference*, 2018.

[12] R. K. Shah and A. L. London, *Laminar flow forced convection in ducts: a source book for compact heat exchanger analytical data*: Academic press, 2014.

[13] J. H. Lienhard, *A heat transfer textbook*: Phlogistron, 2005.

[14] M. Al-Arabi, "Turbulent Heat Transfer in the Entrance Region of a Tube," *Heat Transfer Engineering*, vol. 3, pp. 76-83, 1982/01/01 1982.

[15] V. Gnielinski, "On heat transfer in tubes," *International Journal of Heat and Mass Transfer*, vol. 63, pp. 134-140, 2013.

[16] J. Nonneman, S. Schlimpert, I. T'Jollyn, P. Sergeant, and M. De Paepe, "Experimental Investigation of Direct Contact Baseplate Cooling for Electric Vehicle Power Electronics," in *2019 18th IEEE Intersociety Conference on Thermal and Thermomechanical Phenomena in Electronic Systems (ITherm)*, 2019, pp. 1220-1227.

[17] J. E. Cousineau, K. Bennion, D. DeVoto, M. Mihalic, and S. Narumanchi, "Characterization of Contact and Bulk Thermal Resistance of Laminations for Electric Machines," National Renewable Energy Lab.(NREL), Golden, CO (United States)2015.

[18] L. Siesing, A. Reinap, and M. Andersson, "Thermal properties on high fill factor electrical windings: Infiltrated vs non infiltrated," in *2014 International Conference on Electrical Machines (ICEM)*, 2014, pp. 2218-2223.

[19] T. E. Toolbox. (2019, 26/08/2019). *Material properties for gases, fluids and solids - densities, specific heats, viscosities and more* Available: https://www.engineeringtoolbox.com/material-properties-t_24.html

[20] K. Bennion, "Electric Motor Thermal Management R&D," 2016.

[21] J. D'Errico. (2012). *fminsearchbnd, fminsearchcon*. Available: https://www.mathworks.com/matlabcentral/fileexchange/8277-fminsearchbnd-fminsearchcon